Chinese Chemical Letters 37 (2026) 111483

Contents lists available at ScienceDirect

Chinese Chemical Letters

journal homepage: www.elsevier.com/locate/cclet

In-situ photopolymerization hydrogel bioadhesive for on-demand rapid sealing of kidney wounds

Yaling Wang[a,b,c], Huiting Zhang[b,c], Yu Zhao[a], Mingyang Liu[a], Ming-Jie Yin[b,c,*], Quan-Fu An[b,c], Yansheng Li[a,*]

[a] Department of Urology, Beijing Chao-Yang Hospital, Capital Medical University, Beijing 100020, China
[b] Beijing Key Laboratory for Green Catalysis and Separation, Department of Chemical Engineering, College of Materials Science and Engineering, Beijing University of Technology, Beijing 100124, China
[c] State Key Laboratory of Materials Low-Carbon Recycling, Beijing University of Technology, Beijing 100124, China

ARTICLE INFO

Article history:
Received 14 April 2025
Revised 15 June 2025
Accepted 17 June 2025
Available online 17 June 2025

Keywords:
In-situ photopolymerization
Interface force
Hydrogel bioadhesive
Kidney cancer
Zwitterionic polymer

ABSTRACT

Hydrogel bioadhesives, known for their ability to rapidly inhibit bleeding and minimize damage to surrounding tissues, are revolutionizing traditional surgical procedures. The interfacial force between hydrogel bioadhesives and tissue is critical for achieving strong adhesion in wound healing applications. However, preformed hydrogel bioadhesives cannot achieve seamless closure of irregular shape wounds and tend to detach in bleeding environments, limiting their practical applications. In this study, we developed an *in-situ* photopolymerization hydrogel bioadhesive (IPHB) method to fully seal irregular shape wounds in bleeding conditions within 5 min, eliminating the need for risky artery-blocking procedures. The fluidic hydrogel precursor solution can infiltrate micro- and nanostructured wound, penetrate tissues, and rapidly form an adhesive hydrogel under ultraviolet (UV) irradiation through strong topological entanglement at the interface. The resulting hydrogel demonstrates excellent stretchability, low swelling, and intrinsic antibacterial properties. The IPHB method was successfully employed to seal kidney wounds in a living pig, achieving rapid hemostasis and promoting wound healing without harming healthy tissues. This innovative approach significantly reduces surgical duration and enhances safety. Notably, this study marks the first application of a hydrogel bioadhesive for kidney wound treatment in a living pig, paving the way for safer and more efficient surgical practices.

© 2026 Published by Elsevier B.V. on behalf of Chinese Chemical Society and Institute of Materia Medica, Chinese Academy of Medical Sciences.

The kidney plays a critical role as the body's natural filter, continuously cleansing the blood by removing metabolites through urine. This function is essential for survival, as kidney failure can be life-threatening. In recent years, the incidence of kidney tumors, one of the most common genitourinary cancers, has risen significantly. For instance, in 2019 alone, the economic burden of kidney tumor patients in the United States reached $818 million [1]. Currently, nephron-sparing surgery (NSS) is the standard treatment for early-stage kidney tumors [2]. This surgical approach aims to remove the diseased portion of the kidney while preserving as much healthy tissue as possible. During NSS, the kidney artery is temporarily blocked to minimize bleeding, typically through laparoscopy, with procedures lasting from 30 min to over 1 h [3]. But this prolonged artery occlusion can lead to hypoxic injury of kidney cells. Following tumor excision, suturing is performed to close the incision and prevent postoperative hemorrhage [4]. Besides, suturing requires a 1 cm entry point from the incision edge, inevitably resulting in some loss of healthy kidney tissue. Since kidney tissue does not regenerate, this secondary damage increases the risk of long-term complications and mortality. Therefore, innovative surgical techniques are urgently needed to avoid artery occlusion, ensure effective wound closure, and reduce operation time, ultimately minimizing damage to kidney tissue and improving patient outcomes.

Wound bioadhesives offer a practical and efficient alternative, enabling rapid bleeding control and tissue adhesion without complex procedures like arterial hemostasis. Given that wounds often occur in bleeding environments, it is crucial for these bioadhesives to maintain strong adhesion to tissue in the presence of blood [5–8]. Hydrogels, with their tissue-like structures and tunable adhesive properties, are well-suited for this purpose [9–14]. They promote collagen synthesis and fibroblast proliferation, accelerating epithelialization and wound healing [15–17]. Consequently, hydrogel-based wound bioadhesives offer an innovative alternative

* Corresponding authors.
E-mail addresses: yinmj@bjut.edu.cn (M.-J. Yin), lys-fast@163.com (Y. Li).

https://doi.org/10.1016/j.cclet.2025.111483
1001-8417/© 2026 Published by Elsevier B.V. on behalf of Chinese Chemical Society and Institute of Materia Medica, Chinese Academy of Medical Sciences.

to traditional clinical methods, such as gauze and surgical sutures [18,19]. To achieve strong adhesion in bleeding environments, hydrogels are engineered to first absorb interfacial water and then form contact with tissue surfaces through physical or chemical interactions [20–22]. Nevertheless, conventional hydrogels often absorb excessive water, which weakens their adhesive force and compromises both healing efficiency and durability [23]. To address this limitation, anti-hydration hydrogels with hydrophobic crosslinked chains have been developed [24–26]. These advanced structures minimize water intrusion, preserving strong adhesion even in bleeding conditions. Despite significant advancements in adhesion strength through tailored hydrogel designs, the inherently soft solid state of these materials restricts their ability to conform effectively to wounds with complex geometries [27–29], such as those with wide openings and narrow bases, or narrow openings and wide bases, resulting in the bleeding. In addition, pressure was usually applied when using preformed hydrogels for wounds healing, complexing the surgery steps. This challenge is especially pronounced in laparoscopic procedures, where precise and adaptable wound coverage is critical for effective healing and patient recovery.

Drawing inspiration from the construction industry, where fluid cement is used to seamlessly fill gaps between tiles, we developed a rapid *in-situ* photopolymerization hydrogel bioadhesive (IPHB) method to address these challenges. This approach uses a mixed solution of acrylic acid (AA), zwitterionic monomers, and polyacrylic acid (PAA), analogous to cement solution, that diffuses into the wound area, thoroughly covering it and partially penetrating the tissue (Fig. 1A). As shown in Fig. 1A, upon ultraviolet (UV) irradiation, the solution undergoes *in-situ* photopolymerization [30–32], forming an interpenetrating polymer network (IPN) hydrogel. During polymerization, the polymer chains entangle with the tissue and interact through mechanisms such as strong topological entanglement, hydrogen bonding [33], and electrostatic interactions [34], collectively enhancing adhesion strength. The hydrophilic PAA chains absorb exudative bleeding, while the zwitterionic copolymer network minimizes swelling [35], ensuring stable adhesion in bleeding environments. As shown in Fig. 1B, the reversible physical bonds between the PAA and poly(3-((2-(methacryloyloxy)ethyl)dimethylammonio)propane-1-sulfonate) (PDMAPS) chains confer the hydrogel with stretchability, and the high crosslinking intensity renders its lower swelling. Besides, the zwitterionic feature of the hydrogel promotes the formation of a robust hydration layer to prevent bacterial adhesion, *i.e.*, antibacterial properties [36]. When tested on kidney wounds in a live pig model, the hydrogel bioadhesive demonstrated superior performance compared to traditional suturing, including significantly reduced operation time, simplified procedures, accelerated wound healing, and improved overall safety. This study introduces a groundbreaking approach for kidney wound management, paving the way for safer and more efficient surgical practice, particularly in complex laparoscopic procedures.

As shown in Fig. S1 (Supporting information), the IPN hydrogel is prepared by photopolymerization of AA and DMAPS in the presence of PAA chains with varying DMAPS contents within 200 s. This hydrogel is denoted as PAA-PDMAPS-x, where x represents the DMAPS content. The crosslinking of the PAA-PDMAPS copolymer forms a network structure that is interpenetrated by PAA polymer chains, creating the IPN-structured hydrogel (Fig. 1A). The IPN hydrogel formation process under UV light irradiation is confirmed through *in-situ* monitoring of the precursor solution's state evolution *via* oscillatory shear rheology, as shown in Fig. 1C. Initially, the storage modulus (G') is lower than the loss modulus (G''), indicating the fluidic state of the precursor solution. Upon UV irradiation, both G' and G'' gradually increase, with a sharp three-order magnitude increase observed between 120 s and 150 s. At this point, G'' surpasses G', signifying the transition from a fluid to a solid hydrogel state [37].

Additionally, *in-situ* diffuse reflectance infrared Fourier transform (DRIFT) spectra, shown in Fig. 1D and Fig. S2 (Supporting information), provide further confirmation of the hydrogel formation. These spectra were recorded over 200 s following UV light irradiation, with the characteristic peak intensities increasing over time. Notable peaks include the O–H bending vibration at 3250 cm^{-1},

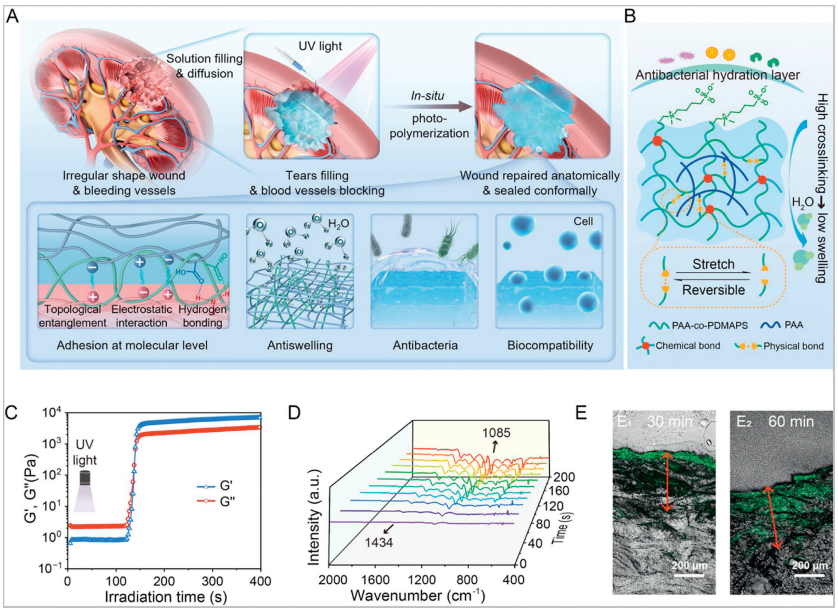


Fig. 1. (A) The scheme for the *in vivo* adaptable sealing the porcine kidney wound *via* rapid *in-situ* photopolymerization of the hydrogel precursor solution method. With the fluidic property of the precursor solution, it could fully cover the whole wound and penetrate deep into the tissue to form strong topological entanglement at the interface, independent of the shape of the wound. (B) Schematic illustration of the mechanisms responsible for the hydrogel's stretchability, antibacterial properties, and low swelling behavior. (C, D) *In-situ* monitoring the conversion of precursor solution into the hydrogel upon UV irradiation *via* the dynamic rheological variation and DRIFT spectra. (E) The depth of the PAA-PDMAPS hydrogel precursor solution penetration into the tissue with different times.

the C–N stretching peak at 1434 cm^{-1}, and the representative $-SO_3^-$ group peaks at 1085 cm^{-1}, all indicating the solid hydrogel's formation. Moreover, Fourier transform infrared (FTIR) spectra for PAA-PDMAPS-x IPN hydrogels (Fig. S3 in Supporting information) demonstrate that the C=O peak intensity increases, while the C=C peak intensity decreases with higher DMAPS content. This reflects the successful polymerization of the monomers and the synthesis of zwitterionic hydrogels. The X-ray photoelectron spectrum (XPS) in Fig. S4 (Supporting information) expresses new peaks for N 1s and S 2p appear for the PAA-PDMAPS-15, further confirming the formation of the copolymer hydrogels. As shown in Fig. S5 (Supporting information), photograph of the fabricated PAA-PDMAPS-x IPN hydrogels are provided in Fig. S5B. These hydrogels exhibit excellent transparency, with over 98 % transmittance in the visible light range (Fig. S5A). The high transparency of the hydrogel allows deep penetration of UV light. For instance, a 3 cm-thick hydrogel can be successfully formed in a mold with opaque surroundings (Fig. S5C), indicating its potential for applications such as sealing kidney wounds, which typically have depths of <2 cm.

Leveraging the IPHB method, the hydrogel precursor solution can freely diffuse throughout the entire area of a cut wound, ensuring comprehensive coverage of every micro- and nanostructure, regardless of the wound's shape. Moreover, the fluidic nature of the hydrogel precursor facilitates partial penetration into the tissue [38]. Upon UV light irradiation, the formed IPN hydrogel chains establish robust topological entanglements with the tissue, ensuring strong adhesion even in bleeding environments (Fig. S6 in Supporting information). This process can be visualized through confocal laser scanning microscopy (CLSM). To assess penetration depth, a fluorophore-modified acrylic acid (FITC-AA) was used as a labeling molecule and co-dissolved with the precursor solution. As shown in Fig. 1E, CLSM images reveal that the hydrogel can form beyond 400 μm beneath the porcine skin surface. This demonstrates that *in-situ* photopolymerized PAA-PDMAPS-x IPN hydrogels overcome the diffusion-limited adhesion typically observed with crosslinked polymers. The resulting strong topological entanglements effectively prevent hydrogel fracture at the interface with porcine skin, highlighting the IPHB method's unique advantages in fabricating hydrogel bioadhesives.

Furthermore, the fluidic properties of the precursors enable PAA-PDMAPS-x IPN hydrogels to rapidly form on irregular shape surfaces and within narrow spaces, an achievement that is difficult for preformed hydrogels but crucial for surgical applications. For demonstration, a round-bottom flask was used to simulate a curved wound requiring sealing through a narrow opening, mimicking the treatment of injuries during minimally invasive surgeries, such as those performed *via* endoscopy (Fig. S7 in Supporting information).

Fig. S8 (Supporting information) highlights the elastic behavior of PAA-PDMAPS-x hydrogels, where G'' consistently exceeds G' within the linear viscoelastic region. This confirms the successful formation of hydrogels with varying DMAPS contents. Furthermore, both G' and G'' increase with DMAPS content, reflecting the mechanical strength enhancement imparted by DMAPS. This improvement arises from the intramolecular electrostatic interactions of the zwitterionic polymers in PDMAPS [39].

Due to these electrostatic interactions, the tensile strain exhibits a significant initial increase, rising from 450 % to 1500 %, a 4-fold enhancement, before declining as DMAPS content exceeds 15 wt% (Figs. S9A and B in Supporting information). The reduction at higher DMAPS concentrations is attributed to decreased water content. This large tensile strain is a critical feature for hydrogel bioadhesives, allowing them to accommodate various deformations and movements [40–43]. Such adaptability is essential for maintaining functionality during everyday human activities. The

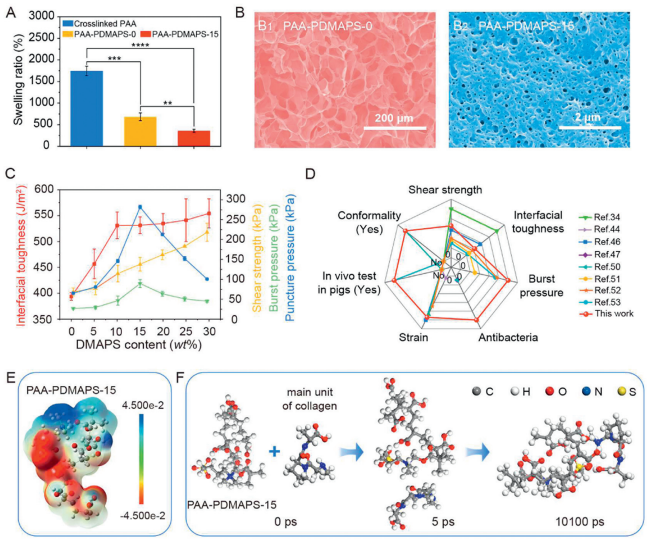


Fig. 2. (A) Swelling ratio variation of hydrogels with and without IPN structures. (B) SEM images of the PAA-PDMAPS-0 (B_1) and PAA-PDMAPS-15 (B_2) IPN hydrogels. (C) Adhesion force of PAA-PDMAPS-x IPN hydrogels with different test methods. (D) Comparison of the wound sealing performance of the PAA-PDMAPS-15 IPN hydrogel with previously reported materials. (E) Electrostatic potential analysis of PAA-PDMAPS-15 IPN hydrogel. (F) Simulation of dynamic interactions between the PAA-PDMAPS-15 IPN hydrogel and the main structural unit of collagen. Data are presented as mean ± SD ($n = 3$). $^{**}P < 0.01$, $^{***}P < 0.001$, $^{****}P < 0.0001$.

stretchability of PAA-PDMAPS-x hydrogels is depicted in Fig. S10 (Supporting information), while the corresponding Young's modulus and toughness are summarized in the Figs. S9C and D (Supporting information). Notably, the hydrogel demonstrates a combination of higher toughness and stretchability alongside a lower Young's modulus, making it well-suited to match the mechanical properties of biological tissues. These features ensure the hydrogel's ability to sustain adhesive performance during diverse activities.

Hydrogels are inherently hydrophilic, enabling them to absorb exudative bleeding effectively. However, excessive swelling can significantly reduce adhesion strength. As shown in Fig. 2A, conventional crosslinked PAA hydrogel bioadhesives exhibit a swelling degree of 1747 %. For an ideal hydrogel bioadhesive, it is crucial to absorb exudative fluids while maintaining minimal swelling to preserve strong adhesion forces.

The incorporation of linear PAA chains reduces the swelling degree, and further increase in DMAPS content leads to a continued decline in swelling, from 684 % for PAA-PDMAPS-0 to 360 % for PAA-PDMAPS-15 IPN hydrogels (Eq. S1 in Supporting information), after 48 h of immersion in simulated body fluid (Fig. 2A). This indicates that the PAA-PDMAPS-x IPN hydrogels effectively mitigate the swelling of PAA hydrogels, demonstrating an anti-swelling effect. This anti-swelling behavior can be attributed to two key factors: (1) The formation of the IPN microstructure, which restricts PAA chain swelling by confining the chains within a tightly entangled network. (2) The electrostatic interactions between PDMAPS and PAA, which reduce the availability of active sites for water absorption. This phenomenon is further supported by the differential scanning calorimetry (DSC) curves of PAA-PDMAPS-x IPN hydrogels (Fig. S11 in Supporting information), where the endothermic peak area decreases with increasing DMAPS content, indicating reduced water content within the IPN hydrogels.

The scanning electron microscopy (SEM) cross-section images in Fig. 2B and Fig. S12 (Supporting information) provide a more obvious evident for the tight microstructure of the PAA-PDMAPS-x IPN hydrogels. The porous structure can be clearly observed, due to the sublimation of water in the hydrogel, which mirrors the

swelling state of the hydrogels. The pore size of PAA-PDMAPS-0 hydrogel is in the range of 50–100 μm, which rapidly diminishes to 0.1–0.2 μm (3 orders decline) for the PAA-PDMAPS-30 IPN hydrogel (the inset of the SEM images presents the pore size distribution). The result illustrates that the swelling degree becomes smaller and the microstructure becomes denser with DMAPS content. It is known that the denser of the microstructure and the smaller of the pores of the polymeric network represent enhanced anti-swelling properties of the hydrogel [44]. In addition, according to previous report, the reduced pore size promotes the cell spreading area, nuclear projection area, and migration speed, which benefits for cell survival [45]. The energy dispersive X-ray spectroscopy (EDS) image in Fig. S12H confirms the uniform distribution of elements throughout the polymeric framework.

The primary factor determining the suitability of PAA-PDMAPS-x IPN hydrogels as wound bioadhesives is their adhesion strength under various conditions. As illustrated in Fig. S13 (Supporting information), the PAA-PDMAPS-15 IPN hydrogel adheres effectively to a variety of materials, including glass, hydrogels, porcine skin, copper, aluminum oxide, and nylon. As shown in Fig. S14 (Supporting information), the adhesion force between the *in-situ*-formed hydrogels and porcine skin was evaluated using multiple *in vitro* test methods, such as the lap-shear test (Fig. S14A), 180-degree peel test (Fig. S14C), puncture test (Fig. S14B), and burst pressure test (Fig. S14D). The results are summarized in Fig. 2C.

The lap-shear test, a widely used method for assessing the adhesion strength of wound dressings (Eq. S2 in Supporting information) [46], shows that the adhesion force increases from 68 kPa for PAA-PDMAPS-0 hydrogel to 218 kPa for PAA-PDMAPS-30 IPN hydrogel (Fig. 2C and Fig. S15 in Supporting information). Notably, the measured fracture force reflects failure within the hydrogel itself, rather than at the interface with porcine skin, indicating that the actual interfacial adhesion force exceeds the measured values (Fig. S16A in Supporting information). Similarly, the 180-degree peel test (Eq. S3 in Supporting information) reveals a comparable trend: the maximum interfacial toughness increases from 394 J/m^2 for PAA-PDMAPS-0 to 531 J/m^2 for PAA-PDMAPS-10 IPN hydrogel, with a further gradual rise for PAA-PDMAPS-30 (Fig. S17 in Supporting information). Once again, fractures occur within the hydrogel, highlighting its robust interfacial adhesion (Fig. S16B in Supporting information).

The high interfacial interaction strength is attributed to the strong topological entanglement achieved *via* the IPHB method and the multifunctional active sites on the PAA-PDMAPS-x IPN hydrogels. The entanglement of polymer chains has been discussed above. Additionally, PAA chains, with a high density of carboxylic acid side chains, interact with tissues *via* electrostatic forces, hydrogen bonding, and other mechanisms. PDMAPS chains, rich in sulfonate, quaternary ammonium, and ester groups, further enhance these interactions [47]. Electrostatic potential analysis (Fig. 2E, Figs. S18D and E in Supporting information) supports this, revealing that PAA-PDMAPS chains exhibit stronger charged features than PAA alone, enabling more effective interactions with collagen and elastin, key tissue components. Dynamic interaction simulations (Fig. 2F and Fig. S18C in Supporting information) confirm that PAA-PDMAPS binds rapidly to the collagen and elastin (Figs. S18A and B in Supporting information) through functional groups such as carboxyl, sulfonate, quaternary ammonium, and ester groups. Notably, the presence of sulfonate and quaternary ammonium groups enhances the interaction forces between the hydrogel and the main structural units of collagen and elastin, increasing from −45.9236 and −49.0018 kcal/mol to −47.5718 and −53.2644 kcal/mol, respectively (Eq. S4 in Supporting information). This explains the enhanced adhesion strength observed with increasing DMAPS content.

For applications such as kidney surgery, where vertical forces predominate after wound sealing, the burst pressure and puncture tests were conducted to simulate real-world conditions. Fig. 2C shows that burst pressure increases with DMAPS content, peaking at 89.3 ± 10.1 kPa for PAA-PDMAPS-15 IPN hydrogel, before declining as DMAPS content exceeds 15 wt%. Similarly, the puncture pressure rises initially, reaching a peak for PAA-PDMAPS-15, before decreasing at higher DMAPS concentrations. Detailed force curves and data (Fig. S19 and Eq. S5 in Supporting information) confirm this trend. The initial increase in burst and puncture pressures is due to the multifunctional interactions of PDMAPS with tissues, enhancing the hydrogel's resistance to external forces. However, at higher DMAPS concentrations, reduced hydrogel stretchability increases its susceptibility to fracturing. Balancing adhesion strength and elongation, the PAA-PDMAPS-15 IPN hydrogel was identified as the optimized formulation for further studies.

Given its intended *in vivo* application, maintaining strong adhesion in biological environments is critical. To evaluate this, wounded porcine skin sealed with PAA-PDMAPS-15 was immersed in simulated body fluid, and adhesion strength was measured over time *via* puncture tests. As shown in Fig. S20 (Supporting information), adhesion force gradually decreases over 48 h but retains >50 % of the original puncture pressure. This performance is attributed to the hydrogel's reduced swelling degree (Fig. 2A).

A critical concern following surgery is the risk of infection, which can significantly hinder wound healing and necessitate the use of antibiotics. Therefore, it is essential to develop wound dressings with inherent antibacterial properties to prevent infections. The PAA-PDMAPS-15 IPN hydrogel, with its zwitterionic features, forms a dense hydration layer on its surface, effectively preventing the nonspecific adsorption of proteins, cells, and microorganisms. The antibacterial property of the hydrogel adhesive was tested against common infection-causing bacteria, including Gram-negative species (*Escherichia coli* (*E. coli*) and *Proteus mirabilis*) and Gram-positive species (*Staphylococcus aureus* (*S. aureus*)).

The antibacterial performance was assessed under various conditions using the inhibition zone method (Figs. 3A and B). In the absence of treatment, the tested paper was surrounded

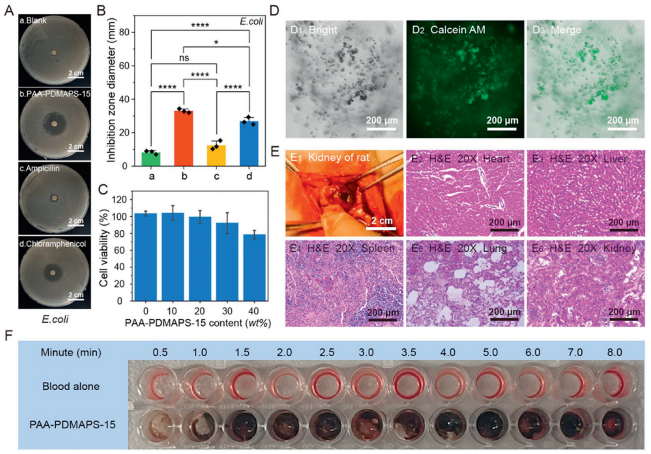


Fig. 3. (A) Photos of the inhibition zones test against *E. coli* with different samples: the blank sample, PAA-PDMAPS-15 IPN hydrogel, ampicillin, and chloramphenicol (from top to bottom). (B) Inhibition zone diameters of the tested samples against *E. coli*: the blank sample (a), PAA-PDMAPS-15 IPN hydrogel (b), ampicillin (c), and chloramphenicol (d). (C) Viability of MOVAS cells cultured with varying concentrations of PAA-PDMAPS-15 IPN hydrogel for 24 h. (D) The scaffold's capacity for MOVAS cell of PAA-PDMAPS-15 IPN hydrogel. (E) *In-situ* photopolymerization of the PAA-PDMAPS-15 IPN hydrogel for sealing rat kidney wounds, along with H&E staining of major organs one week post-treatment. (F) Coagulation assay for the PAA-PDMAPS-15 IPN hydrogel. Data are presented as the mean ± SD ($n = 3$). $^{*}P < 0.05$, $^{****}P < 0.0001$.

by a dense growth of *E. coli*. However, the PAA-PDMAPS-15 IPN hydrogel exhibited strong antibacterial activity, creating an inhibition zone with a diameter of 33.0 ± 1.2 mm. This performance surpassed that of commonly used antibiotics, with inhibition zones of 12.4 ± 2.6 mm for ampicillin and 26.9 ± 2.2 mm for chloramphenicol. Additionally, the hydrogel demonstrates inhibitory effects against *S. aureus* and *Proteus mirabilis* (Fig. S21 in Supporting information). These results highlight the hydrogel's potent antibacterial activity against both Gram-positive and Gram-negative bacteria. The remarkable antibacterial activity of the hydrogel originates from the formation of a hydration layer, which serves as a physical barrier against bacterial adhesion [48].

The biosafety of both the hydrogel precursor solution and the corresponding PAA-PDMAPS-15 IPN hydrogel was evaluated using standard cell counting kit-8 (CCK-8) assays (details are given in Supporting information). The viability of mouse aortic vascular smooth muscle cells (MOVAS) was assessed after 24 h of culture in media containing various concentrations of the hydrogel (Fig. 3C) and its precursor solutions (Fig. S22 in Supporting information). Results indicated that MOVAS cells maintained over 80% viability across all tested concentrations for both materials, demonstrating compliance with international biomaterial safety standards (ISO 10993:2009) [49]. Notably, as shown in Fig. 3D, MOVAS cells adhered well on the PAA-PDMAPS-15 IPN hydrogel, further confirming its excellent biosafety profile.

Moreover, the hemostatic properties of the PAA-PDMAPS-15 IPN hydrogel are critical for effective wound sealing. To evaluate this, an *in vitro* coagulation assay was performed. As shown in Fig. 3F, the hydrogel rapidly induced thrombosis, demonstrating excellent hemostatic performance.

Compared to previous works, the PAA-PDMAPS-15 IPN hydrogel adhesive exhibits superior performance across multiple metrics (Fig. 2D) [34,44,46,47,50–53]. It achieves the highest burst pressure, excellent antibacterial properties, enhanced interfacial toughness, increased conformality, and the unique ability to completely seal irregular shape wounds. These exceptional characteristics make the hydrogel adhesive highly suitable for sealing various wound types and rapidly stopping bleeding, a critical requirement for laparoscopic operations. In addition, as given in Table S1 (Supporting information), compared with the preformed hydrogel bioadhesives, the topological entanglement by the IPHB method endows the hydrogel bioadhesives with superior interfacial interaction strength, *i.e.*, up to 218 kPa of shear strength, 531 J/m^2 of interfacial toughness, and 89.3 kPa of burst pressure. As a result, the fabricated PAA-PDMAPS-x IPN hydrogel bioadhesive realized rapid and robust adhesion to various substrates without additional pressure.

The IPHB method was subsequently applied to seal kidney wounds in rats (Fig. 3E). After one week of post-operative feeding following standard procedures, major organs were harvested for histological evaluation using H&E staining. As shown in Fig. 3E, no abnormalities were observed in the heart, liver, spleen, lungs, or kidneys. These results confirm the good biocompatibility of the PAA-PDMAPS-15 IPN hydrogel.

The PAA-PDMAPS-15 IPN hydrogel was utilized for sealing NSS wounds on porcine kidneys due to its excellent adaptability to various wound shapes, strong adhesion, flexibility, antibacterial properties, and remarkable biocompatibility. To ensure its safety, initial tests were conducted on the kidney wound of a freshly deceased pig. As illustrated in Fig. S23 (Supporting information), the hydrogel precursor was successfully photopolymerized *in-situ* within 5 min, effectively sealing the wound. Encouraged by these results, this convenient technique was subsequently applied to kidney wounds in a living pig. Animal care and experimental protocols were approved by the Ethics Committee of Beijing

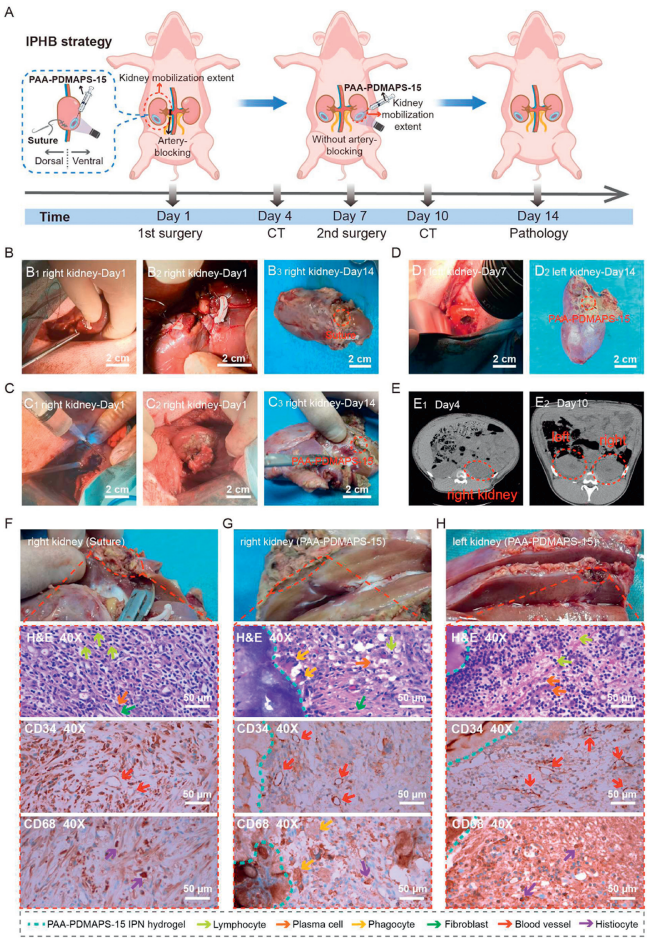


Fig. 4. (A) Timeline for the simulation of NSS and sealing the wounds with the PAA-PDMAPS-15 IPN hydrogel. Photos of the NSS: (B) sealing the wound of porcine right kidney with traditional suture technique; (C) sealing the wound of porcine right kidney with the PAA-PDMAPS-15 IPN hydrogel *via in-situ* photopolymerization; and (D) sealing the wound of porcine left kidney with the PAA-PDMAPS-15 IPN hydrogel *via in-situ* photopolymerization. (E) CT scan of the pig abdomen after sealing with the PAA-PDMAPS-15 IPN hydrogel after 4 days (E_1) and 10 days (E_2). Pathology of porcine kidneys including H&E staining and immunohistochemical staining against CD34 and CD68 after 2-week sealing: (F) the right kidney sealed with suture method; (G) the right kidney sealed with the PAA-PDMAPS-15 IPN hydrogel; and (H) the left kidney sealed with the PAA-PDMAPS-15 IPN hydrogel.

Chao-Yang Hospital, Capital Medical University, China (approval No. 2023–3–30–6).

As shown in Fig. 4A, two wounds measuring 2 cm in diameter and 1 cm in depth are created on the right kidney of the living pig. These wounds were sealed using two different methods: The traditional suture technique and the innovative IPHB method. Both methods are performed under temporary blockage of the kidney artery with a clamp to prevent bleeding. The artery-blocking procedure requires 20–30 min, while the suture and IPHB techniques take 20 and 5 min to seal the wound, respectively (Figs. 4B and C). Three days post-operation, an abdominal computed tomography (CT) scan (Fig. 4E) reveals no abnormalities or bleeding in or around the right kidney. However, the traditional suture procedure requires 40–50 min and relies on a skilled surgeon to minimize the risk of kidney tissue damage. In contrast, the IPHB method completes the operation in 25–35 min, saving approximately 15 min. Moreover, the speedy merit of the IPHB strategy can be more obvious in laparoscopic operation. These findings highlight that the IPHB strategy offers a rapid, straightforward, and highly safe ap-

proach for kidney wound therapy, presenting a promising alternative to the traditional suture method.

Building on its high efficiency in stopping bleeding, the IPHB strategy was further applied to seal kidney wounds in a living pig without occluding the kidney artery. One week after the initial surgery, a second wound measuring 1.5 cm in diameter and 1 cm in depth was created on the pig's left kidney (Fig. 4A). Notably, the bleeding during this second procedure was more significant than that in the first operation. Impressively, the PAA-PDMAPS-15 IPN hydrogel bioadhesive, applied using the IPHB strategy, rapidly stopped the bleeding (Fig. 4D and Fig. S6), underscoring its strong hemostatic capability. Moreover, this strategy can be applied on any irregular shape wound surface that demands for sealing. An abdominal CT scan conducted three days after the surgery (Fig. 4E) revealed no abnormalities or bleeding in or around the kidneys, demonstrating the hydrogel bioadhesive's exceptional wound-sealing performance. Furthermore, no abnormalities or bleeding was observed in the right kidney, further validating the hydrogel's effectiveness. Importantly, the entire surgical procedure does not require occlusion of the kidney artery, significantly reducing the operation time to under five min and lowering the skill demands on the operator. This is especially valuable in emergency situations. And the pig remained in good health following the surgery.

Two weeks after surgery, the kidneys were excised for examination. As shown in Figs. 4B–D, no hematoma was observed around either kidney, accenting the hydrogel's excellent sealing performance. Remarkably, the hydrogel remains firmly adhered to the wound even after two weeks in the internal body environment. This durable adhesion is attributed to topological entanglement and multiple physical interactions between the hydrogel and surrounding tissues.

To evaluate wound healing efficiency, microscale observation techniques were used to examine the healed wounds treated with either standard sutures or the PAA-PDMAPS-15 IPN hydrogel after one and two weeks. Hematoxylin-eosin (H&E) staining, as shown in Figs. 4F and G, provides a clear visualization of the tissue at the wound sites in porcine kidneys, with the blue line marking the edge of the PAA-PDMAPS-15 IPN hydrogel. Initial granulation tissue is evident in wounds treated with both methods. Notably, the intensity of inflammatory cells in wounds treated with the IPHB method is comparable to that of standard sutures, indicating similar wound dressing efficacy. By the 14th day after right kidney NSS, lymphocytes, plasma cells, and fibroblasts is observed in both treatment groups.

As shown in Figs. 4F–H, the PAA-PDMAPS-15 IPN hydrogel group exhibits significantly more CD34- and CD68-positive cells in the granulation tissue compared to the suture group. This finding confirms the hydrogel's capability to enhance the wound healing efficiency of kidney wounds, highlighting the advantages of IPHB method in promoting kidney wound healing. Although biodegradability is not a requirement for applications such as partial nephrectomy, the degradation performance of the PAA-PDMAPS-15 IPN hydrogel was still studied in Fig. S24 (Supporting information), which shows slight degradation in 8-day test.

These results demonstrate that the IPHB strategy enables the *in-situ* formation of strong topological entanglements, significantly enhancing the interfacial interaction between the hydrogel bioadhesive and tissue. Consequently, it achieves rapid hemostasis within 5 min, effectively promoting wound healing under bleeding conditions, without causing additional damage to surrounding tissues or increasing the risk of infection. Therefore, this IPHB approach holds great potential to transform traditional suturing methods.

In conclusion, we proposed an IPHB method to rapidly construct PAA-PDMAPS-x IPN hydrogel bioadhesive for irregular shape wounds, providing effective hemostasis and promoting wound healing. Thanks to its fluidic properties, the hydrogel precursor can diffuse into tissue and form topological entanglements at the molecular level upon UV irradiation, resulting in exceptional adhesion strength even in bleeding environments. By optimizing the DMAPS content, the PAA-PDMAPS-15 IPN hydrogel was identified as the most effective formulation, offering remarkable stretchability and strong adhesion. Furthermore, its zwitterionic nature endowed it with significant antibacterial properties, effectively inhibiting the main bacterial strains found in the urinary tract. Notably, the IPHB method was successfully applied to treat kidney wounds in a living pig model, simulating surgical conditions. The results demonstrated that this method achieved similar outcomes to standard suturing surgery, with faster healing, simplified procedures, reduced operation time, and enhanced safety. Thus, the proposed IPHB method presents a promising alternative to traditional suturing for kidney wound healing. Moreover, it has the potential to be extended to other partial resections of solid organs, such as the liver and spleen.

Declaration of competing interest

The authors declare that they have no known competing financial interests or personal relationships that could have appeared to influence the work reported in this paper.

CRediT authorship contribution statement

Yaling Wang: Writing – original draft, Investigation, Formal analysis, Data curation. **Huiting Zhang:** Software, Data curation. **Yu Zhao:** Formal analysis. **Mingyang Liu:** Formal analysis. **Ming-Jie Yin:** Writing – review & editing, Supervision, Methodology, Funding acquisition, Formal analysis. **Quan-Fu An:** Writing – review & editing, Supervision, Funding acquisition. **Yansheng Li:** Writing – review & editing, Supervision, Funding acquisition, Data curation.

Acknowledgments

This work was financially supported by the National Natural Science Foundation of China (Nos. 22278010, 22125801) and Beijing Hospitals Authority Clinical medicine Development of special funding support (No. YGLX202304).

Supplementary materials

Supplementary material associated with this article can be found, in the online version, at doi:10.1016/j.cclet.2025.111483.

References

[1] E.J. Schafer, A. Jemal, D. Wiese, et al., Eur. Urol. 84 (2023) 117–126.
[2] K. Kieran, A.M. Davidoff, Pediatr. Surg. Int. 31 (2015) 229–236.
[3] R. Cabello, J.V. Garcia, C. Quicios, et al., Adv. Surg. Tech. 27 (2017) 715–716.
[4] F. Porpiglia, R. Bertolo, D. Amparore, C. Fiori, Eur. Urol. Focus. 5 (2019) 600–603.
[5] Z. Wang, X. Wan, S. Wang, Chem 9 (2023) 771–783.
[6] C. Cui, W. Liu, Prog. Polym. Sci. 116 (2021) 101388.
[7] X. Chen, X. Zhang, S. Yang, et al., Chin. Chem. Lett. 36 (2025) 110021.
[8] S. Zhang, H. Zhou, C. Huang, et al., Chin. Chem. Lett. 33 (2022) 4321–4325.
[9] G. Liu, Z. Bao, J. Wu, Chin. Chem. Lett. 31 (2020) 1817–1821.
[10] L. Xie, X. Zhang, X. Wang, et al., Chin. Chem. Lett. 36 (2025) 110848.
[11] X. Liu, M. Shen, T. Bing, et al., Adv. Sci. 11 (2024) 2402208.
[12] Y. Liu, T. Zhu, M.J. Yin, J. Li, Z. Yin, Innovation 6 (2025) 100736.
[13] S. Cheng, M. Pan, D. Hu, et al., Chin. Chem. Lett. 34 (2023) 108276.
[14] X. Li, L. Guan, X. Li, et al., Chin. Chem. Lett. 36 (2025) 110661.
[15] Y. Liang, X. Zhao, T. Hu, et al., Small 15 (2019) 1900046.
[16] C. Huang, Z. Zhang, Y. Fang, et al., Int. J. Biol. Macromol 278 (2024) 134496.
[17] G. Liu, Y. Zhou, Z. Xu, et al., Chin. Chem. Lett. 34 (2023) 107705.
[18] S. Luo, L. Yang, Q. Zou, et al., Chem. Eng. J. 472 (2023) 144865.
[19] J. Zhao, P. Qiu, Y. Wang, et al., Int. J. Biol. Macromol. 244 (2023) 125250.
[20] C. Gao, D. Zheng, B. Long, et al., Eur. Polym. J. 201 (2023) 112590.
[21] Y.N. Fu, Y. Li, B. Deng, et al., Bioact. Mater. 8 (2022) 165–176.

[22] Y. Wang, Z. Yuan, Y. Pang, et al., ACS Appl. Mater. Interfaces 15 (2023) 20661–20676.
[23] J. Zhu, Y. Li, W. Xie, et al., ACS Appl. Mater. Interfaces 14 (2022) 53575–53592.
[24] Y. Liang, H. Xu, Q. Han, et al., Nano Today 54 (2024) 102105.
[25] H. An, M. Zhang, Z. Huang, et al., Adv. Mater. 36 (2024) 2310164.
[26] S. Bian, L. Hao, X. Qiu, et al., Adv. Funct. Mater. 32 (2022) 2207741.
[27] Y. Zhao, Z. Dai, H. Huang, J. Tian, H. Cai, Appl. Biochem. Biotechnol. 197 (2025) 821–836.
[28] X. Liu, J. Hu, Y. Hu, et al., Colloids Surf. B 245 (2025) 114346.
[29] T. Hu, G.P. Wu, H. Bu, et al., Chem. Eng. J. 450 (2022) 138201.
[30] Z.R. Li, T.R. Lv, Z. Yang, et al., Chem. Eng. J. 484 (2024) 149375.
[31] J.Y. Zhang, T.R. Lv, Y.H. Xue, et al., Chem. Eng. J. 495 (2024) 153510.
[32] Q. Liu, W. Wang, H. Yang, et al., Adv. Funct. Mater. 34 (2024) 2406376.
[33] S.J. Wu, X. Zhao, Chem. Rev. 123 (2023) 14084–14118.
[34] G. Tian, D. Yang, C. Liang, et al., Adv. Mater. 35 (2023) 2212302.
[35] J. Ren, G. Chen, H. Yang, et al., Adv. Mater. 36 (2024) 2412162.
[36] C. Leng, S. Sun, K. Zhang, S. Jiang, Z. Chen, Acta Biomater 40 (2016) 6–15.
[37] S.M. Magami, R.L. Williams, J. Appl. Polym. Sci. 135 (2018) 46691.
[38] S. Nam, D. Mooney, Chem. Rev. 121 (2021) 11336–11384.
[39] H. Liu, C. Xiong, Z. Tao, et al., RSC Adv. 5 (2015) 33083–33088.
[40] H. Yuk, B. Lu, X. Zhao, Chem. Soc. Rev. 48 (2019) 1642–1667.
[41] X. Peng, X.F. Xia, X.Y. Xu, et al., Sci. Adv. 7 (2021) eabe8739.
[42] M.J. Yin, Z. Yin, Y. Zhang, Q. Zheng, A.P. Zhang, Nano Energy 58 (2019) 96–104.
[43] M.J. Yin, M. Yao, S. Gao, et al., Adv. Mater. 28 (2016) 1394–1399.
[44] L. Li, M. Yue, Q. Peng, X. Pu, Z. Li, Adv. Funct. Mater. 34 (2023) 2309594.
[45] J. Xia, Z.Y. Liu, Z.Y. Han, et al., Acta Biomater. 141 (2022) 178–189.
[46] H. Yuk, C.E. Varela, C.S. Nabzdyk, et al., Nature 575 (2019) 169–174.
[47] J. Yan, Y. Ji, M. Huang, et al., ACS Mater. Lett. 2 (2020) 1375–1380.
[48] Y. Zhang, Y. Ding, X. Li, et al., Chin. Chem. Lett. 32 (2021) 3636–3640.
[49] A. Rungrod, A. Kapanya, W. Punyodom, et al., Biomacromolecules 22 (2021) 3839–3859.
[50] X. Xie, X. Jin, B. He, et al., Appl. Mater. Today 27 (2022) 101477.
[51] S.J. Wu, J. Wu, S.J. Kaser, et al., Nat. Commun. 15 (2024) 1215.
[52] K. Shen, Z. Lv, Y. Yang, et al., Adv. Mater. 37 (2025) 2414092.
[53] P. Ma, W. Liang, R. Huang, et al., Adv. Mater. 36 (2024) 2305400.